



LAWRENCE
LIVERMORE
NATIONAL
LABORATORY

Distinguishing mechanisms of morphological instabilities in phase change materials during switching

M. K. Santala, S. Raoux, T. Topuria, B. W. Reed,
T. Lagrange, G. H. Campbell

April 10, 2014

Thin Solid Films

Disclaimer

This document was prepared as an account of work sponsored by an agency of the United States government. Neither the United States government nor Lawrence Livermore National Security, LLC, nor any of their employees makes any warranty, expressed or implied, or assumes any legal liability or responsibility for the accuracy, completeness, or usefulness of any information, apparatus, product, or process disclosed, or represents that its use would not infringe privately owned rights. Reference herein to any specific commercial product, process, or service by trade name, trademark, manufacturer, or otherwise does not necessarily constitute or imply its endorsement, recommendation, or favoring by the United States government or Lawrence Livermore National Security, LLC. The views and opinions of authors expressed herein do not necessarily state or reflect those of the United States government or Lawrence Livermore National Security, LLC, and shall not be used for advertising or product endorsement purposes.

Distinguishing mechanisms of morphological instabilities in phase change materials during switching

M.K. Santala^{1,a}, S. Raoux^{2,b}, T. Topuria³, B.W. Reed¹, T. LaGrange¹, G.H. Campbell¹

¹Condensed Matter and Materials Division, Lawrence Livermore National Laboratory, 7000 East Ave., Livermore, CA 94551, USA

²IBM T.J. Watson Research Center, 1101 Kitchawan Rd., Yorktown Heights, NY 10598, USA

³IBM Research - Almaden, 650 Harry Rd., San Jose, CA 95120, USA

The process of dewetting of a thin film from a solid substrate is important for its scientific and technological relevance, but can be difficult to observe experimentally. We report on an experimental method that may be used to investigate morphological changes, including dewetting, during laser heat treatment of alloys used for phase change memory devices. We have used nanosecond-scale time-resolved imaging to differentiate between competing thin film instabilities in GeTe, a chalcogenide-based phase change material. It is shown that in the absence of nucleated dewetting, thin films of phase change alloys may be unstable, but that nucleated dewetting can lead to a more disrupted final state of the thin film.

The thermal stability of thin films and nanostructures is important for performance and reliability of materials for many applications, including memory based on phase change materials (PCMs). Chalcogenide-based PCMs, such as Ge₂Sb₂Te₅ and GeTe, are important for

^a Author to whom correspondence should be addressed. Electronic mail: santala1@llnl.gov

^b Current address: Helmholtz-Zentrum Berlin für Materialien und Energie GmbH, Berlin, Germany

use in optical recording media and non-volatile resistance-based memory devices,¹ which exploit the distinct optical and electrical properties of the amorphous and crystalline phases. For memory applications, switching between the amorphous and crystalline phases is achieved within a few nanoseconds by laser or Joule heating.¹ During crystallization the amorphous PCM may be heated well above its glass transition temperature and during amorphization the melting temperature of the crystalline PCM is exceeded.^{2,3} Heating induces an increase in atomic mobility which enables rapid phase transformations, but which can also induce morphological changes adversely affecting device performance and reliability. Some studies⁴⁻⁶ have addressed device reliability by observing changes in microstructure and nanostructure morphology during heat-induced phase switching. Morphology changes leading to void formation have been observed in electrically-switched GeTe nanowires.⁵ Morphological defects have been observed in in-line PCM cells due to faceting of grains during crystallization of the amorphous phase.⁶ AFM experiments show that during a full switching cycle (crystal to amorphous to crystalline) the topography of a PCM thin film may not return to its original shape.⁴

Although morphology changes can have a dramatic effect on the performance of PCM devices,^{5,6} relatively few studies of the physical mechanisms underlying morphology changes and dewetting have been published about PCMs. This may be, in part, due to the short timescales (ns) under which these morphological changes occur in PCMs when rapidly heated by laser or Joule heating, making the relevant experimental measurements difficult to accomplish. The processes leading to hole formation in thin films of Te and Ge-Te alloys have been considered by Kivits *et al.*⁷ in the context of intentional hole formation for optical data storage. They considered how gradients in surface tension and pressure induced by localized laser heating may lead to film thinning and rupture at the center of the laser-affected area and also considered the

role of defects and pre-existing film defects in hole formation. The aforementioned mechanisms may play a role in the development of thickness variations and hole formation during laser amorphization and crystallization in thin films of $\text{Ge}_2\text{Sb}_2\text{Te}_5$ shown in Figure 1. However, the patterns of the thickness variations in Figure 1a and b and the more complex patterns of laser-induced thickness changes observed with *in situ* TEM during laser crystallization of amorphous GeTe thin films⁸ suggest that other types of thin films instabilities may be operational. Here we report on initial results using nanosecond time-resolved TEM to investigate the physical mechanisms causing thin film instabilities in PCM thin films during laser annealing.

Thin film instabilities and dewetting have been studied very extensively in other material systems,^{9-14,15-17,18-21} due to their importance in an enormous range of technologies (e.g. paints, coatings, electronics, dielectric layers, thermal barrier coatings, etc.). Instabilities and dewetting in liquid thin films can be initiated in several ways.⁹⁻¹¹ They may begin at pre-existing defects, such as pinholes, or may be nucleated¹¹ by a local variation in surface tension or film pressure which cause local thinning of the film. Instabilities can be induced by van der Waals interactions requiring no nucleation event.^{9,12} It has been shown that in free-standing⁹ or supported¹² very thin liquid films (<100nm), thickness fluctuations above a critical wavelength, λ_c , will grow spontaneously due to the disjoining pressure arising from van der Waals interactions (below λ_c the film is still effectively stabilized by surface tension). The wavelength of the thickness fluctuation with the fastest growing amplitude, $\lambda_m = \sqrt{2}\lambda_c$, determines the characteristic length scale of the instabilities.^{9,12} Instabilities caused by van der Waals interactions are sometimes called “spinodal” instabilities because the mathematical analysis is formally analogous to the analysis of the more familiar chemical spinodal decomposition.¹² Nucleated and spinodal dewetting may be simultaneously active as shown for liquid thin films of polymers,¹⁵ metals¹³

and collagen solutions.¹⁶

PCMs are generally embedded in a larger device or at least capped with a material that remains solid during the rapid heating used to induce the phase transformation, e.g. the ultrathin amorphous silicon nitride layer in Figure 1c. The presence of a solid capping layer on the PCM introduces another layer of complexity. Capping layers change the physical interactions, such as interfacial energies and van der Waals interactions, and introduce new factors, such as mechanical properties and stress state, in the solid capping material.^{20,21} The presence of a solid cap may suppress some instabilities^{19,21} but, if subject to compressive stresses, may induce instabilities.^{17,21} The need to better understand the complex physical mechanisms causing instabilities in nanostructured PCMs during switching motivates experimental observations of their development during laser heating in an effort to distinguish the different mechanisms of instability development.

We observe the development of morphological instabilities *in situ*, on the nanosecond scale, in capped GeTe films during laser heat treatment. GeTe is an important PCM, because its high crystallization temperature, T_x , relative to other commonly used PCMs^{22,23} and rapid switching speed^{23,24} make it attractive for random access memory applications. GeTe has been the subject of numerous theoretical and experimental studies including several examining the crystallization behavior of amorphous thin films during isothermal²⁵ and laser^{2,3} heating and morphological changes have been seen during switching of GeTe nanowires.⁵ Here we focus on GeTe, but we have observed similar instabilities in similarly prepared and treated $\text{Ge}_2\text{Sb}_2\text{Te}_5$ and GaSb thin films.

In situ observations allow us to differentiate dewetting mechanisms that would be difficult to distinguish in *post mortem* analysis. The microstructural changes that occur during laser heating

would be impossible to observe with most *in situ* imaging techniques because they occur on the nanosecond to microsecond time scale and on a nanometer length scale. We use the dynamic TEM (DTEM), a pulsed photoemission TEM at Lawrence Livermore National Laboratory, to image the GeTe during the development of morphological instabilities. The DTEM achieves nanosecond-scale time-resolved imaging of irreversible processes in condensed phases with intense photo-emitted electron pulses. During a time-resolved experiment, a reaction is initiated in the specimen with a “pump” laser pulse. A pulse from another laser, which is timed against the pump laser pulse in an operator-defined delay, strikes the cathode inducing a burst of $\sim 10^{10}$ photoemitted electrons, enough to form an image or diffraction pattern of a transient state of the material. The duration of the electron pulse passing through the reacting specimen defines the temporal resolution of the experiment. The DTEM has been used to study laser-induced crystallization in PCMs,^{3,8,26} rapidly-driven phase transformations in metals²⁷ and semiconductors,²⁸ and has been used to verify that spinodal dewetting is the controlling physical mechanism in the dewetting of ultrathin liquid Ni films.²⁹ The design and operation of the DTEM have been described elsewhere.³⁰

Morphological instabilities were induced by laser-heating as-deposited amorphous films of 30 nm GeTe on a Si support with a 20 nm thick amorphous silicon nitride window (0.25 x 0.25 mm) and 8 nm silica capping layer. GeTe was deposited at room temperature using magnetron sputtering. A target with a nominal composition of Ge:Te = 50:50 atomic % was used. Rutherford backscattering spectrometry revealed the film composition to be Ge 50.7 ± 2.0 atomic % and Te 49.3 ± 2.0 atomic %. The specimen was heated with a Nd:YAG laser (1064 nm wavelength, 135 ± 5 - μm $1/e^2$ diameter, 12-ns FWHM pulse duration). The spot size on the specimen is larger than practical for memory devices, but the large, uniformly thick heated area

is ideal for making observations that allow differentiation between different dewetting mechanisms. Laser heating was induced with pulses having energies ranging from 4.0 to 5.2 μJ . The higher energies were used to allow the area of the specimen within the field of view to remain fluid for hundreds of nanoseconds, allowing thickness variations and dewetting to develop to a degree that they could be more easily observed. Bright-field TEM images generated from 15-ns electron pulses were recorded before, during, and after laser heat treatment. The electron probe pulses and pump laser were aligned such that area where the specimen received the greatest laser intensity was imaged. Selected areas of laser-treated specimens were cut with a focused ion beam (FIB) to form thin cross-sections for *post-mortem* imaging in a conventional TEM.

Direct temperature measurements are not experimentally accessible for most laser heating experiments, but temperatures have been modeled.³ Spatio-temporal temperature profiles caused by laser-specimen interactions and heat flow were developed using a commercially available finite element analysis (FEA) modeling software (COMSOL Multiphysics) the details of which are available in the supplemental material of reference [3]. Simulations of temperatures at the center of the laser spot where the specimens were imaged are shown in Figure 2. The temperature rises rapidly during the laser pulse, but the cooling (governed by two-dimensional heat conduction in the suspended thin film) takes many microseconds. Heating due to the enthalpy of crystallization is not included in the model; it has been estimated that this could locally increase the temperature by $\sim 180\text{K}$ near the crystallization front.³

Figure 3 shows morphological changes developing during crystallization of GeTe induced by a 4.0 μJ laser pulse. The development of the thickness variations occurs simultaneously with crystallization and the development of a hole, which was most likely nucleated at a pre-existing

defect such as an impurity inclusion. The thickness variations run roughly parallel to the grain boundaries of four large GeTe grains at the top and center of Figure 3c and perpendicular to the circular rim of a dewet region in the lower right corner of the image. The morphology of the thickness variations was confirmed by TEM imaging of focused ion beam (FIB) cross sections (Figure 3d). The silicon nitride membrane forming the window of the Si TEM grid remained flat and the thickness variations in the GeTe that developed with distinctly regular, sinusoidal character were accommodated by displacement of the silica capping layer which remained conformal to the GeTe. In this case, in addition to the morphological changes, there are concomitant processes, *e.g.* phase transformations with accompanying changes in volume and crystal structure.

To allow observation of instabilities in the absence of crystallization, higher laser energies were used and 15-ns images were taken 500 ns after peak laser exposure of the specimen. Since the amorphous material is heated to higher temperatures, the nucleation rate of the crystalline phase at the center of the laser spot remains very low and the amorphous phase remains fluid for hundreds of nanoseconds. Note that although the simulated temperatures in Figure 2 are below the melting temperature (997K) of crystalline GeTe, it has been shown that the amorphous solid may transition to a liquid phase at temperatures well below the melting temperature of the crystalline phase.⁸ Figure 4 (a,c,e,g) show GeTe 500 ns after laser exposure for several laser energies. The same areas are shown minutes later in conventional TEM images (b,d,f,h). Instabilities of different types are seen to develop. The images in Figure 4 are 512 × 512 pixel selections capturing the area heated by the center of the laser spot; the uncropped versions are available in the Supplemental Material.³¹

Circular holes in the GeTe grow in Figure 4 (a,e); they are likely nucleated at inclusions in

the films that are visible at the center of the holes in these time resolved images. Dewetting may have nucleated at these points either because of a local increase in temperature from increased laser absorption at the defects or due to a change to the energetic barrier to nucleation, i.e. alteration of the balance of the interfacial energies. The nucleated hole in Figure 4a has a larger radius in the image taken after crystallization (4b); the crystallization of the film presumably halted the further retraction of the edge of the hole. In addition to the nucleated hole, the 4.3 μJ laser shot caused regular thickness variations (Fig. 4b) that are not visible yet at 500 ns. The direction of the thickness variations appears to be biased by the nucleated hole as in the example shown in Figure 3c.

Figure 4 (c, g) show time resolved images of thin film instabilities in the absence of nucleated holes. Thickness variations in both cases are already apparent at 500 ns after laser heating. In the final, *post mortem* crystallized microstructures (Fig. 4 (d, h)) both the amplitude and the wavelength of the thickness variations are significantly greater than at 500 ns. For the 5.2 μJ laser shot, the amplitude of the thickness variations increased to the point that the GeTe dewet in the troughs of the film leaving bare lines on the silicon nitride support. A fast Fourier transform (FFT) was taken of each image (Fig. 4 insets). The peak intensity of each rotationally averaged FFT in the pulsed images was taken as a measure of the characteristic wavelength, λ_m , of the instability at 500 ns after laser heating. At 500 ns, λ_m was found to be 320 nm and 290 nm for the 5.2 μJ and 4.6 μJ shots, respectively. The amplitude of the instabilities for the 4.2 μJ is too small at 500 ns to measure λ_m . In the images of the final microstructure, the wavelength of the thickness variations has coarsened to 500 nm, 500 nm, and 390 nm at the time of crystallization for the 5.2 μJ , 4.6 μJ , and 4.2 μJ shots respectively. The coarsening of the wavelength may be driven by capillary effects unrelated to the mechanisms initiating the

instability, so having measurements in the early stages of morphological development is important.

We have made estimates of λ_m produced either purely by van der Waals forces or by mechanical destabilization (see Supplemental Materials³¹). The estimate for van der Waals driven instabilities is $\sim 140 \mu\text{m}$ and for a mechanical buckling instability in the solid capping film it is $0.8 \mu\text{m}$. Both estimates are larger than the wavelength of the instabilities observed here, but the estimate for the van der Waals induced instabilities is off by more than two orders of magnitude, while the estimate for mechanical instabilities is within a factor of three. This strongly suggests that mechanical instabilities are more important in the driving the non-nucleated thin films instabilities in this system, though it does not exclude an influence of van der Waals forces. From these initial experimental results, we are unable to quantify the relative influence of the van der Waals forces and mechanical (de)stabilization of the solid capping film on the λ_m in this system given the complexity of their interactions.²¹ However, it has been shown for uncapped polystyrene that by varying the liquid film and substrate thickness, different mechanisms of thin film instabilities may be distinguished.¹⁸ Since the van der Waals and mechanical forces scale differently with changing thickness of the fluid and capping layers, similar experiments to differentiate the relative importance of these mechanisms are possible. Since the characteristic amplitude, wavelength, and growth rate of linearized models of non-nucleated thin film instabilities apply to the earliest stages of film breakup,^{9,12,21} characterization and kinetic data from the early stages of development is necessary¹⁵ and the nanosecond time-resolved *in situ* experiments described here will be instrumental in this characterization.

As a final observation, the behavior the GeTe film after $5.0 \mu\text{J}$ laser pulse is distinctly different from what occurs for higher ($5.2 \mu\text{J}$) and lower ($4.6 \mu\text{J}$) energy laser shots. The

behavior may appear anomalous if only the final microstructure is observed, but the time-resolved images give great insight in explaining the apparently anomalous behavior. The nucleated dewetting initiates very soon after laser heating and by 500 ns some of the circular patches bare of GeTe are more than 2 μm in diameter. It is the early development of the bare patches and the rapid retraction of the edges of the GeTe film that leads to a more advanced final state of dewetting. The final state consists of isolated drops of GeTe. Nucleated dewetting results in a more disrupted final state of the thin film compared to the results from purely non-nucleated dewetting at similar laser energies because of the earlier pinch-off of the GeTe film. It is useful to note however that non-nucleated dewetting may have a similar final microstructure, *c.f.* Figures 4 (e,f) and 4 (a,b), thus the *in situ* experiments allow differentiation of dewetting mechanisms that may not be obvious from *post mortem* characterization.

We have imaged thin amorphous PCM in the time between laser heating and crystallization to capture early stages of morphological instabilities. The dewetting develops both from nucleation of bare patches and from spinodal instabilities. Although the spinodal instabilities may arise from either van der Waals interactions or a mechanical instabilities, the length scale of the observed instabilities during early stages of development indicate that mechanical instabilities are more important for driving the early stages of instabilities in these experiments. Further experiments are planned to quantify the relative importance of mechanical stresses and van der Waals forces in the destabilization of PCM thin films.

ACKNOWLEDGMENTS

This work performed under the auspices of the U.S. Department of Energy, Office of Basic Energy Sciences, Division of Materials Sciences and Engineering by Lawrence Livermore National Laboratory under Contract DE-AC52-07NA27344. We thank P. Tchoulfian for

performing ex-situ laser experiments and E.A. Delenia for preparation of the FIB cross section.

REFERENCES

- ¹ S. Raoux and M. Wuttig, *Phase Change Materials: Science and Applications*. (Springer Verlag, Berlin, 2009).
- ² E. Huber and E. E. Marinero, *Phys. Rev. B* **36**, 1595 (1987).
- ³ M. K. Santala, B. W. Reed, S. Raoux, T. Topuria, T. LaGrange, and G. H. Campbell, *Appl. Phys. Lett.* **102**, 174105 (2013).
- ⁴ V. Weidenhof, I. Friedrich, S. Ziegler, and M. Wuttig, *J. Appl. Phys.* **86**, 5879 (1999).
- ⁵ S. Meister, H. Peng, K. McIlwrath, K. Jarausch, X. F. Zhang, and Y. Cui, *Nano Letters* **6**, 1514 (2006).
- ⁶ B. J. Kooi, J. L. M. Oosthoek, M. A. Verheijen, M. Kaiser, F. J. Jedema, and D. J. Gravesteijn, *Physica Status Solidi B-Basic Solid State Physics* **249**, 1972 (2012).
- ⁷ P. Kivits, R. Debont, B. Jacobs, and P. Zalm, *Thin Solid Films* **87**, 215 (1982).
- ⁸ M. K. Santala, B. W. Reed, S. Raoux, T. Topuria, T. LaGrange, and G. H. Campbell, *Physica Status Solidi B-Basic Research* **249**, 1907 (2012).
- ⁹ A. Vrij and J. T. Overbeek, *Journal of the American Chemical Society* **90**, 3074 (1968).
- ¹⁰ F. Brochard Wyart and J. Daillant, *Canadian Journal of Physics* **68**, 1084 (1990).
- ¹¹ H. S. Kheshgi and L. E. Scriven, *Chemical Engineering Science* **46**, 519 (1991).
- ¹² V. S. Mitlin, *J. Colloid Interface Sci.* **156**, 491 (1993).
- ¹³ J. Bischof, D. Scherer, S. Herminghaus, and P. Leiderer, *Physical Review Letters* **77**, 1536 (1996).
- ¹⁴ A. Oron, S. H. Davis, and S. G. Bankoff, *Reviews of Modern Physics* **69**, 931 (1997); S. Herminghaus, K. Jacobs, K. Mecke, J. Bischof, A. Fery, M. Ibn-Elhaj, and S. Schlagowski, *Science* **282**, 916 (1998); A. Sharma and R. Khanna, *Physical Review Letters* **81**, 3463 (1998).
- ¹⁵ R. Xie, A. Karim, J. F. Douglas, C. C. Han, and R. A. Weiss, *Physical Review Letters* **81**, 1251 (1998).
- ¹⁶ U. Thiele, M. Mertig, and W. Pompe, *Physical Review Letters* **80**, 2869 (1998).
- ¹⁷ N. Bowden, S. Brittain, A. G. Evans, J. W. Hutchinson, and G. M. Whitesides, *Nature* **303**, 146 (1998); N. Sridhar, D. J. Srolovitz, and Z. Suo, *Appl. Phys. Lett.* **78**, 2482 (2001).
- ¹⁸ R. Seemann, S. Herminghaus, and K. Jacobs, *Physical Review Letters* **86**, 5534 (2001).
- ¹⁹ R. Huang and Z. Suo, *J. Appl. Phys.* **91**, 1135 (2002).
- ²⁰ P. J. Yoo and H. H. Lee, *Physical Review Letters* **91** (2003).
- ²¹ R. Huang and Z. Suo, *Thin Solid Films* **429**, 273 (2003).

- ²² S. Raoux, B. Munoz, H.-Y. Cheng, and J. L. Jordan-Sweet, *Appl. Phys. Lett.* **95**, 143118 (2009).
- ²³ G. Bruns, P. Merkelbach, C. Schlockermann, M. Salinga, M. Wuttig, T. D. Happ, J. B. Philipp, and M. Kund, *Appl. Phys. Lett.* **95**, 043108 (2009).
- ²⁴ M. Chen, K. A. Rubin, and R. W. Barton, *Appl. Phys. Lett.* **49**, 502 (1986); S. Raoux, H. Y. Cheng, M. A. Caldwell, and H. S. P. Wong, *Appl. Phys. Lett.* **95**, 071910 (2009).
- ²⁵ Q. M. Lu and M. Libera, *J. Appl. Phys.* **77**, 517 (1995); A. M. Mio, E. Carria, G. D'Arrigo, S. Gibilisco, M. Miritello, M. G. Grimaldi, and E. Rimini, *Journal of Non-Crystalline Solids* **357**, 2197 (2011); A. Bastard, J. C. Bastien, B. Hyot, S. Lhostis, F. Momprou, C. Bonafos, G. Servanton, C. Borowiak, F. Lorut, N. Bicaïs-Lepinay, A. Toffoli, C. Sandhya, A. Fantini, L. Perniola, E. Gourvest, S. Maitrejean, A. Roule, V. Sousa, D. Bensahel, and B. Andre, *Appl. Phys. Lett.* **99**, 243103 (2011).
- ²⁶ M. K. Santala, B. W. Reed, T. Topuria, S. Raoux, S. Meister, Y. Cui, T. LaGrange, G. H. Campbell, and N. D. Browning, *J. Appl. Phys.* **111**, 024309 (2012).
- ²⁷ T. LaGrange, G. H. Campbell, P. E. A. Turchi, and W. E. King, *Acta Materialia* **55**, 5211 (2007); J. S. Kim, T. LaGrange, B. W. Reed, M. L. Taheri, M. R. Armstrong, W. E. King, N. D. Browning, and G. H. Campbell, *Science* **321**, 1472 (2008); J. S. Kim, T. LaGrange, B. W. Reed, R. Knepper, T. P. Weihs, N. D. Browning, and G. H. Campbell, *Acta Materialia* **59**, 3571 (2011); A. Kulovits, J. M. K. Wiezorek, T. LaGrange, B. W. Reed, and G. H. Campbell, *Philosophical Magazine Letters* **91**, 287 (2011); J. McKeown, A. Kulovits, C. Liu, K. Zwiack, B. W. Reed, T. LaGrange, J. M. K. Wiezorek, and G. H. Campbell, *Acta Materialia* **65**, 56 (2014).
- ²⁸ L. Nikolova, T. LaGrange, B. W. Reed, M. J. Stern, N. D. Browning, G. H. Campbell, J. C. Kieffer, B. J. Siwick, and F. Rosei, *Appl. Phys. Lett.* **97**, 203102 (2010); L. Nikolova, T. LaGrange, M. J. Stern, J. M. MacLeod, B. W. Reed, H. Ibrahim, G. H. Campbell, F. Rosei, and B. J. Siwick, *Phys. Rev. B* **87** (2013).
- ²⁹ J. T. McKeown, N. A. Roberts, J. D. Fowlkes, Y. Wu, T. LaGrange, B. W. Reed, G. H. Campbell, and P. D. Rack, *Langmuir* **28**, 17168 (2012).
- ³⁰ M. R. Armstrong, K. Boyden, N. D. Browning, G. H. Campbell, J. D. Colvin, W. J. DeHope, A. M. Frank, D. J. Gibson, F. Hartemann, J. S. Kim, W. E. King, T. B. LaGrange, B. J. Pyke, B. W. Reed, R. M. Shuttlesworth, B. C. Stuart, and B. R. Torralva, *Ultramicroscopy* **107**, 356 (2007); B. W. Reed, M. R. Armstrong, N. D. Browning, G. H. Campbell, J. E. Evans, T. LaGrange, and D. J. Masiel, *Microscopy and Microanalysis* **15**, 272 (2009).
- ³¹ See supplemental material at [*URL to be inserted by AIP*].

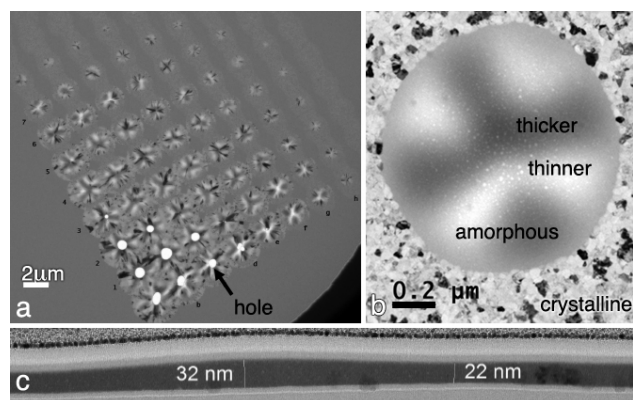


Figure 1. Conventional ex-situ TEM images of (a) laser-crystallized marks in an amorphous $\text{Ge}_2\text{Sb}_2\text{Te}_5$ thin film and (b) a laser-amorphized mark in a crystalline film. Within the amorphous mark, darker areas are thinner and lighter areas thicker. High-angle annular dark field scanning TEM of the area in 1b (see Supplemental Material³¹) and (c) TEM of a FIB cross section of a laser-amorphized area, similar to that shown in (b), confirm the contrast changes in the amorphous region are due to thickness variations. Similar thickness variations occur within the crystalline marks and holes develop in the $\text{Ge}_2\text{Sb}_2\text{Te}_5$ with increased laser energy and pulse duration ((a),

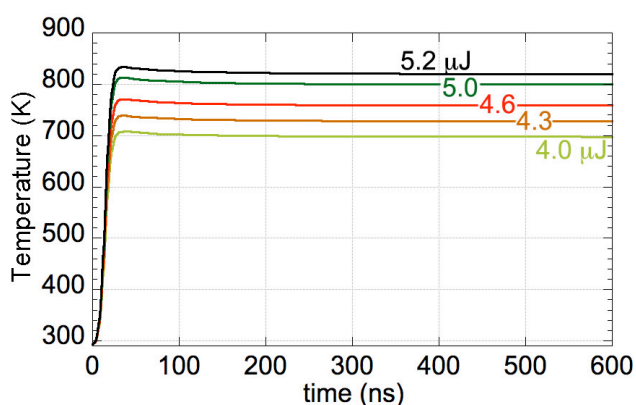


Figure 2 Simulated temperature during 1064-nm wavelength laser heating of silica-capped GeTe on a $250\ \mu\text{m}$ silicon nitride TEM window. The temperatures plotted are for the point at the center of the Gaussian laser pulse and are given for the range of energies used in the experiments. Heating is rapid during the first few nanoseconds while the laser is on. After the laser pulse the local temperature remains steady for microseconds.

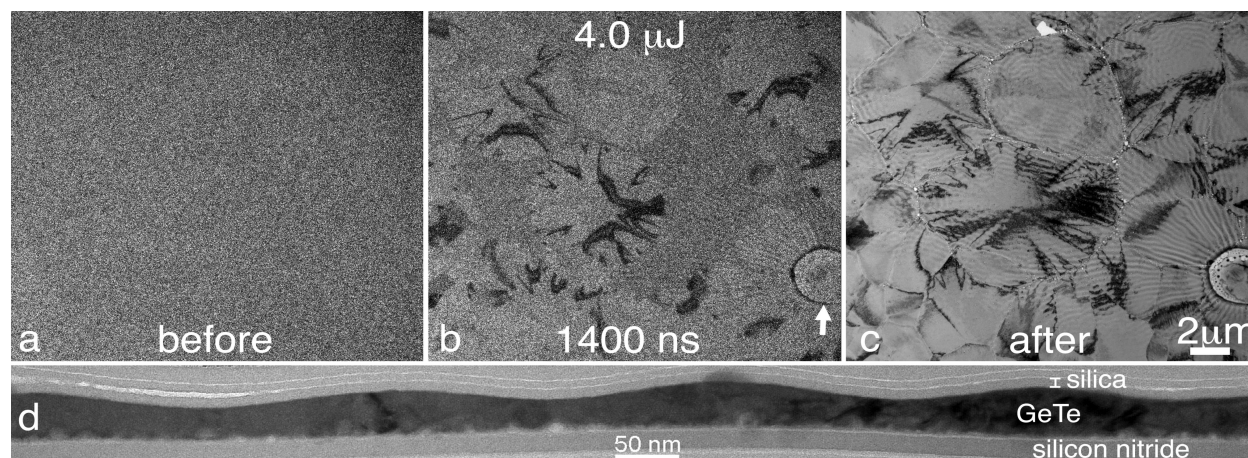


Figure 3 TEM images show morphological instabilities and dewetting in a laser crystallized GeTe thin film. The as-deposited 30 nm GeTe film (a) appears featureless. A 15-ns pulsed electron image 1400 ns after the peak in laser heating (b) shows crystalline grains (lighter ovals with very dark bend contours) growing into the amorphous film. The arrow marks dark circular edge of an area that has partially dewet. The same region is shown minutes later in a conventional image (c), the evenly spaced light and medium grey striations radiating from the circular flaw in the lower right and running parallel to the grain boundaries in the large grains in the center of the image are due to thickness variations. A TEM image of a focused ion beam cross section (d) of the film confirms the striations are due to thickness variations and shows their regular sinusoidal morphology.

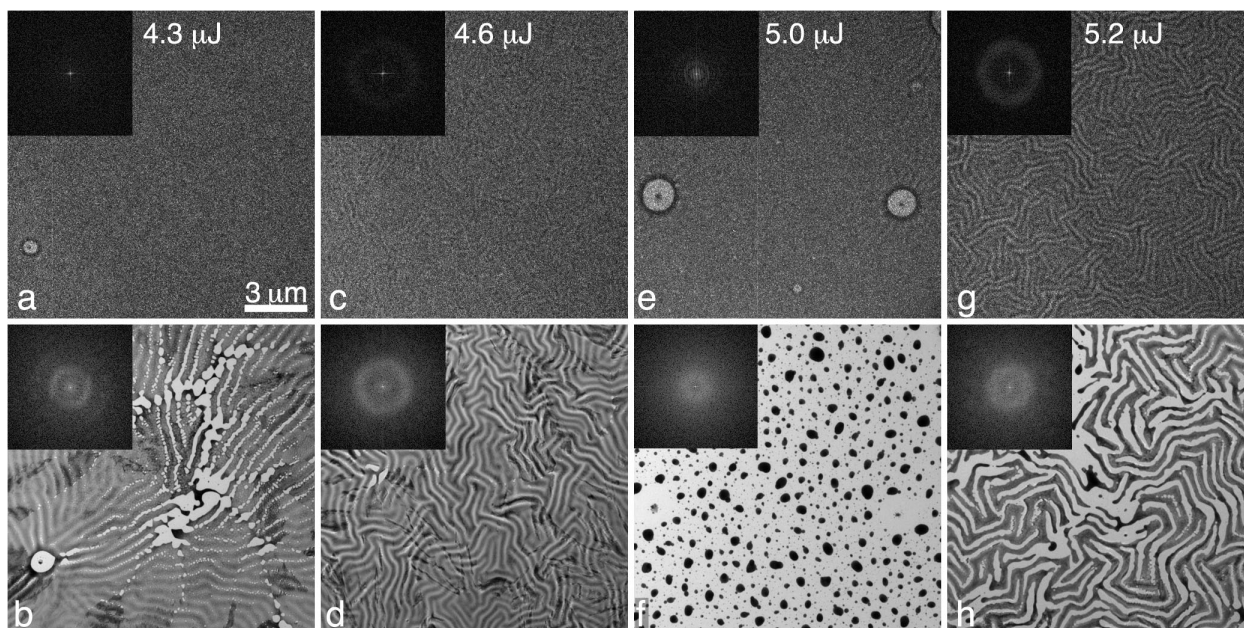


Figure 4 Time-resolved (15 ns) images of GeTe films 500 ns after laser exposure for four different laser energies (top row). The same areas were imaged minutes after laser exposure using conventional bright field imaging (bottom row). All images are to the same scale. Insets are FFT-generated power spectra. Images and spectra have been cropped; see the Supplemental Material³¹ for uncropped versions.

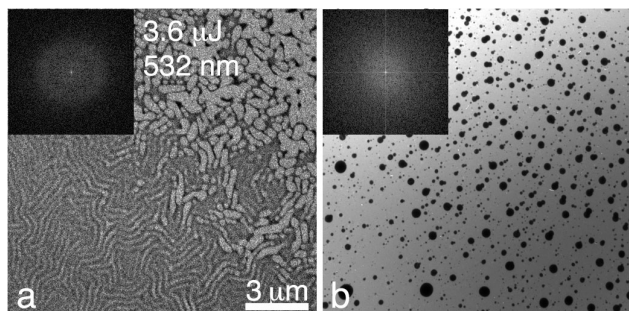


Figure 5 Dewetting 500 ns after a 532 nm laser pulse (a) and the same are minutes later (b). The dewetting appears to occur through a non-nucleated spinodal process but the final microstructure appears similar to figure 4f, where nucleated dewetting appeared to control morphological development. *In situ* characterization distinguishes mechanisms not apparent in *post mortem* characterization. The laser energy is lower than in Fig 4 but GeTe absorbs more in the green than in the ultraviolet part of the spectrum.

SUPPLEMENTAL MATERIAL to

**DISTINGUISHING MECHANISMS OF MORPHOLOGICAL INSTABILITIES IN
PHASE CHANGE MATERIALS DURING SWITCHING**

by M.K. Santala, S. Raoux, T. Topuria, B.W. Reed, T. LaGrange, G.H. Campbell

Scanning Tem (STEM) Image of an Amorphous Mark in $\text{Ge}_2\text{Sb}_2\text{Te}_5$

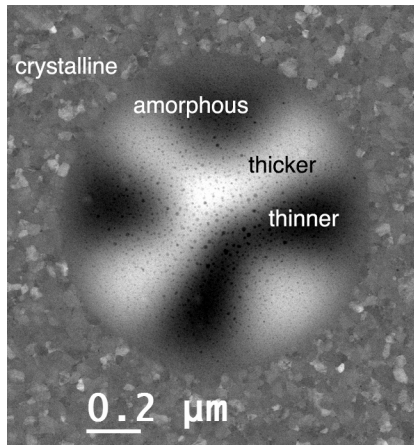


Fig. S1. High-angle annular dark field (HAADF) STEM image of the amorphous mark picture in Figure 1b of the main text. HAADF STEM is especially sensitive to the atomic number and thickness of the specimen. Here the changes in contrast within the amorphous spot confirm the changes in thickness.

Uncropped Images and Spectra in Figure 4 of the Main Text

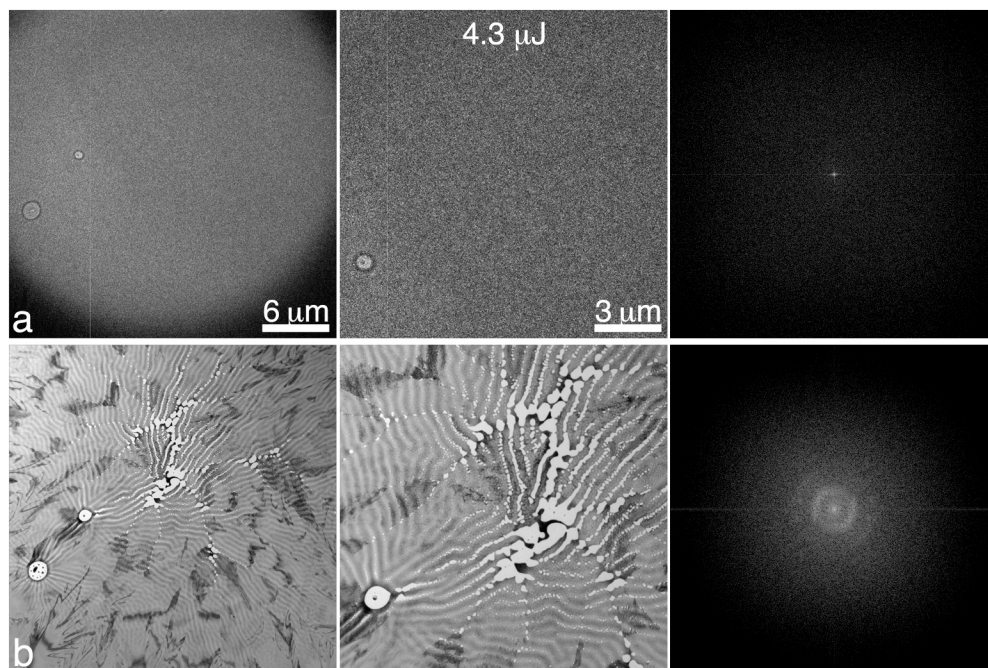


Fig. S2. Uncropped versions of the images in Figure 4 a and b of the main text (left). The 512×512 pixel selections shown in the main text (center). Uncropped FFT-generated power spectra of the 512×512 pixel selections (right).

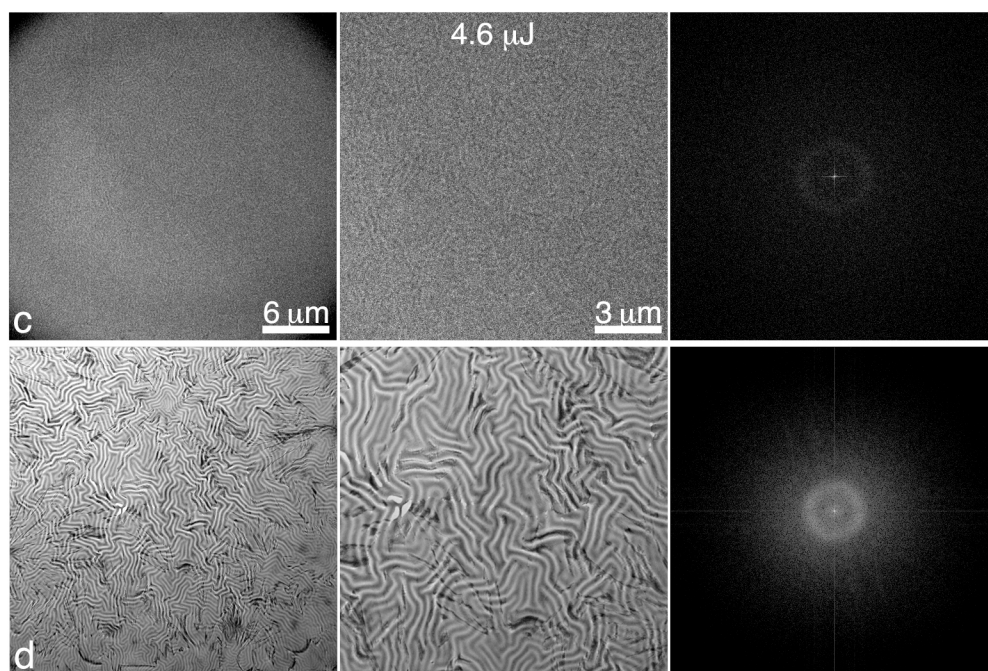


Fig. S3. Uncropped versions of the images in Figure 4 c and d of the main text (left). The 512×512 pixel selections shown in the main text (center). Uncropped FFT-generated power spectra of the 512×512 pixel selections (right).

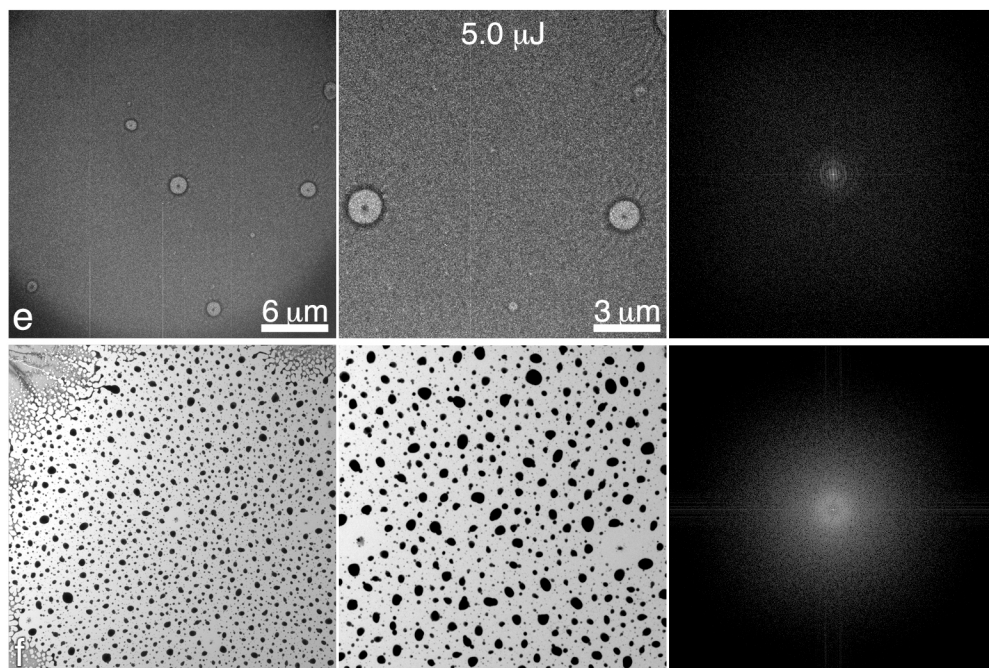


Fig. S4. Uncropped versions of the images in Figure 4 e and f of the main text (left). The 512×512 pixel selections shown in the main text (center). Uncropped FFT-generated power spectra of the 512×512 pixel selections (right).

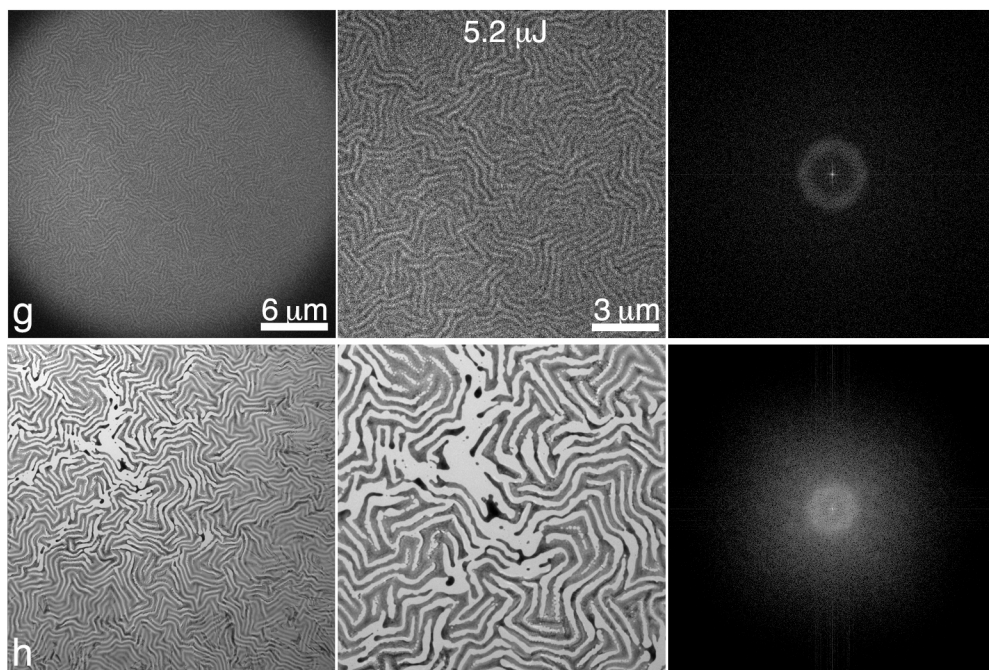


Fig. S5. Uncropped versions of the images in Figure 4 g and h of the main text (left). The 512×512 pixel selections shown in the main text (center). Uncropped FFT-generated power spectra of the 512×512 pixel selections (right).

Uncropped Versions of Images and Spectra in Figure 5 of the Main Text

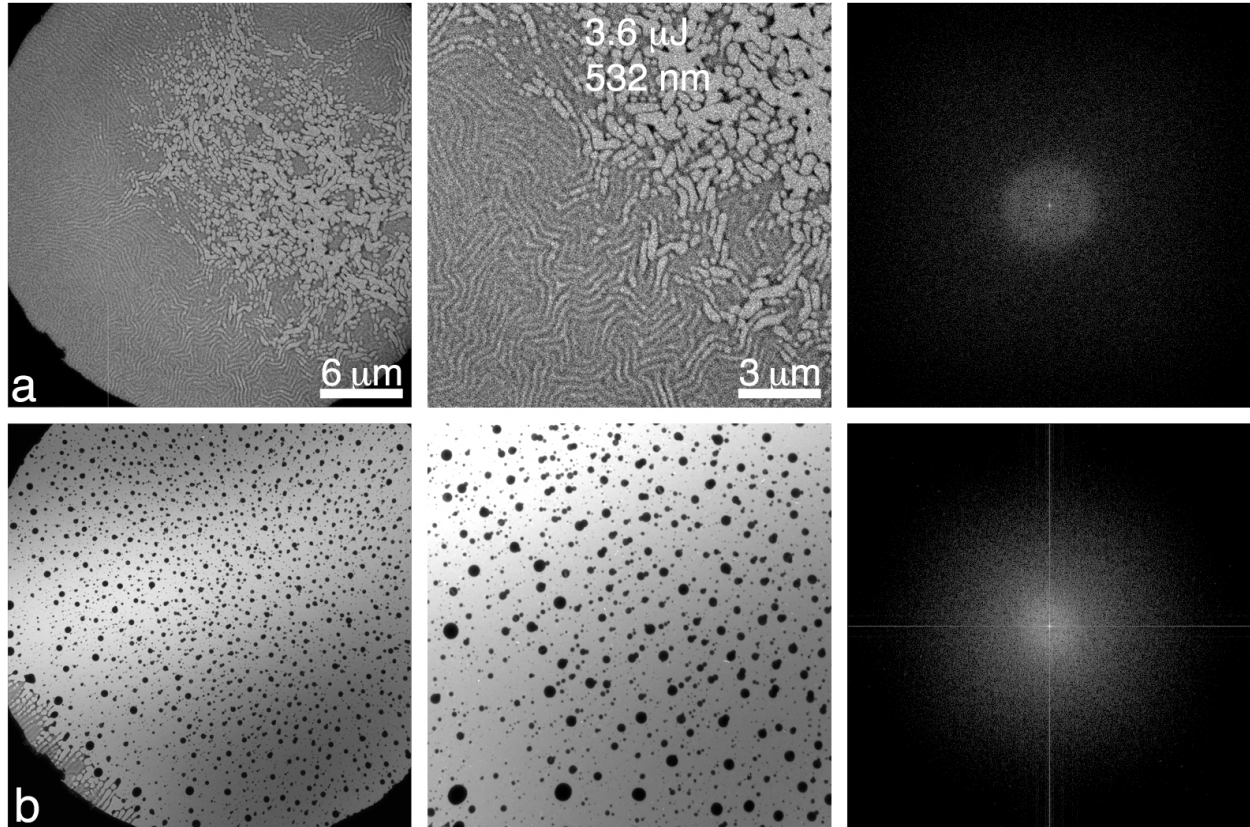


Fig. S6. Uncropped versions of the images in Figure 5 a and b of the main text (left). The 512×512 pixel selections of the original images shown in the main text (center). Note that in this case only, the 512×512 pixel selection does not coincide with the exact center of the laser heated area. This was to allow some of the thickness variations to be within the field of view of the cropped figure that appears in the main text. Uncropped FFT-generated power spectra of the 512×512 pixel selections (right).

Estimation of Characteristic Wavelength of Instabilities

The characteristic wavelength, λ_m , or the wavelength that has the maximum growth rate of its amplitude, is estimated here for two cases of instabilities: (1) instabilities arising purely from van der Waals interactions and (2) instabilities arising purely from a mechanical instability due to compressive stresses developed in the solid capping layer during laser heating.

From Vrij and Overbeek,¹ we estimate λ_m due to van der Waals interactions:

$$\lambda_{m,vdW} = \sqrt{\frac{8\pi^3\gamma h^4}{A}} \quad (i)$$

where γ is the interfacial energy, h is the initial thickness of the GeTe layer, and A is the effective Hamaker constant. The Hamaker constant for two media interacting across a third condensed medium (here the support and capping materials interacting across the GeTe) will vary with the polarizability of the materials but is expected to be on the order of 10^{-20} J for most materials.² Using $h = 30$ nm for the GeTe film thickness and representative values of $\gamma = 1$ J/m² and $A = 10^{-20}$ J, yields $\lambda_{m,vdW} = 140$ μ m, orders of magnitude off from the ~ 0.30 μ m observed.

For the mechanical stresses, we assume that the silicon nitride membrane may be treated as a rigid support; the supports used are under tensile stress and remain relatively flat even during the development of significant thickness variations in the GeTe as seen in the cross section images, *c.f.* Figure 1d (main text). We assume that the amorphous capping layer initial is stress free and that in the regions where the GeTe has been heated adequately to flow like a liquid, the capping layer buckles to accommodate compressive stresses that develop due to laser heating.

From Sridhar *et al.*,³ we estimate the characteristic buckling wavelength of a solid thin film on a viscous layer due to compressive stress. For limit of a thin viscous layer the characteristic wavelength is:

$$\lambda_{m,mech} = \frac{2\pi h_{cap}}{\sqrt{\frac{2}{3}12\varepsilon_o(1+\nu)}} \quad (\text{ii})$$

where h_{cap} is the thickness of the solid capping layer, ε_o is the strain in the solid thin film, and ν is the Poisson ratio of the solid film. We use the properties of fused silica to make our estimates: $\nu = 0.17$ and a coefficient of thermal expansion $5.5 \times 10^{-7}/^\circ\text{C}$ to estimate the strain for a change in temperature of 500°C . For a capping layer thickness of 8 nm we find $\lambda_{m,mech}$ to be 0.8 μm , larger than the observed wavelength of the thickness variations, but within a factor of three. This rough estimate assumes the initial stress in the deposited film is negligible. If (as is likely for an 8 nm thick film deposited on thicker free-standing films of dissimilar materials) this is not the case, then $\lambda_{m,mech}$ may be significantly shorter than 0.8 μm .

Both the van der Waals and mechanical instability estimates are larger than the wavelength of the instabilities observed here. Since both estimates are simplified views of a complex process that could include both mechanisms, and since only representative values were taken for some physical parameters in the models, it is not surprising that neither estimate for matches the experimental observations perfectly. However, the estimate for the van der Waals induced instabilities is off by more than two orders of magnitude, while the estimate for mechanical instabilities is within a factor of three. This very strongly suggests that mechanical instabilities are more important in initially driving the non-nucleated thin film instabilities in this system, though it does not exclude an influence of van der Waals forces.

References for Supplemental Material

- ¹ A. Vrij and J. T. Overbeek, *Journal of the American Chemical Society* **90**, 3074 (1968).
- ² J. Isrealachvili, *Intermolecular and Surface Forces*. (Elsevier Ltd., London, 1991).
- ³ N. Sridhar, D. J. Srolovitz, and Z. Suo, *Appl. Phys. Lett.* **78**, 2482 (2001).